J. Biochem. **142,** 201–211 (2007)
doi:10.1093/jb/mvm130

RVCaB, a Calcium-binding Protein in Radish Vacuoles, is Predominantly an Unstructured Protein with a Polyproline Type II Helix

Jun Ishijima[1,†], Nahoko Nagasaki[2,†], Masayoshi Maeshima[2,*] and Masashi Miyano[1,*]

[1]Structural Biophysics Laboratory, RIKEN SPring-8 Center, Harima Institute, Kouto, Sayo, Hyogo, 679-5148; and [2]Laboratory Cell Dynamics, Graduate School of Bioagricultural Sciences, Nagoya University, Nagoya, 464-8601, Japan

Received March 8, 2007; accepted May 21, 2007; published online June 16, 2007

A unique acidic calcium-binding protein RVCaB, rich in glutamic acid and proline and lacking aromatic amino-acid residues, exists in radish vacuoles, and is thought to be involved in the vacuole Ca^{2+}-storage function. In the present study, we focused on the protein physicochemical properties of RVCaB to understand its uniqueness in terms of structure and Ca^{2+}-binding function. On differential scanning calorimetry, the protein did not show any sharp transition of heat-denaturation of the folded protein except for a gradual excess of heat capacity when heated up to 99°C from 20°C. The Ca^{2+}-binding ability of RVCaB was retained after heat treatment. No α-helix or β-sheet was detected in the far-UV CD spectra of RVCaB as judged by several computer programs for protein structure analysis. However, further analyses with CD spectroscopy suggest that RVCaB has a left-handed polyproline type II (PPII) helix, which is known to be in a collagen chain conformation. The number of Ca^{2+} bound to RVCaB was determined to be 21.6, and a 360 M^{-1} *Ka* value for Ca^{2+} binding was determined by isothermal titration calorimetry. The analysis also revealed that the binding of Ca^{2+} to RVCaB is an entropy-driven phenomenon. We prepared tryptophan-inserted mutants of RVCaB (V136W and V202W) to probe the Ca^{2+}-induced structural change by fluorescent spectroscopy. The analysis suggests a small structural rearrangement of RVCaB upon Ca^{2+}-binding and that the induced Trp residues at 136 and 202 are exposed to solvent in each mutant. These results suggest that RVCaB does not have a definitive protein fold except for the extended PPII structure and that its structure changes slightly by the binding of Ca^{2+} or heat treatment. These findings suggest that the unique structure of RVCaB with its PPII helices is closely related to its high-capacity and low-affinity Ca^{2+}-binding properties.

Key words: calcium-binding protein, circular dichroism, unstructured protein, polyproline type II helix.

Abbreviations: CaBP, calcium-binding protein; DSC, differential scanning calorimetry; ITC, isothermal titration calorimetry; PPII, poly(L-proline) type II; RVCaB, radish vacuolar calcium-binding protein.

Some natively unfolded or intrinsically unstructured proteins (often abbreviated as 'IUPs') have been reported (*1–4*), whereas the amino-acid sequence of proteins encoded by genes is thought to possess all the information necessary to adopt the definitive native 3D structure needed to function (*5*). The particular features of the amino acid sequence responsible for the lack of the definitive structure have been analysed (*6–13*). Dunker *et al*. (*7*) suggested that 10% of the unstructured proteins were metal-binding proteins with a structure suitable for such binding. At the present, however, there is no report of such a protein whose structure is unrelated to its metal-binding property.

We reported a new type of calcium-binding protein (CaBP), radish vacuolar calcium-binding protein (RVCaB), which localizes in the vacuoles of radish taproots (*14*), where the vacuoles are a major Ca^{2+}-storage organelle, which stores Ca^{2+} in a millimolar range (1−10 mM) in plant cells (*15*, *16*). RVCaB may exert a Ca^{2+} buffer to the uptake of such a high concentration of Ca^{2+} in vacuoles, since the Ca^{2+} concentration is maintained in a micro-molar in the cytosol as a second messenger (*14*). In fact, the expression of the RVCaB gene is regulated in response to exogenous Ca^{2+} (*14*, *17*), and the RVCaB may contribute to the signal transduction network. However, there is no similar sequence motif in the RVCaB amino-acid sequence of weakly conserved four time repeats to those of the other known CaBPs, including the EF-hand proteins such as calmodulin, annexin and calreticulin (*14*). The unique amino acid sequence of RVCaB with 248 residues is rich in glutamic acid (33%),

*To whom correspondence should be addressed. Tel: +81-791-58-2815, Fax: +81-791-58-2816, E-mail: miyano@spring8.or.jp or maeshima@agr.nagoya-u.ac.jp or
†These two authors contributed equally to this work.

valine, lysine and proline, but has no aromatic amino acids as well as no cysteine, glycine, asparagine or arginine (*14*). These properties of the RVCaB sequence could be a good fit with that of the intrinsically unstructured proteins (IUP) (*18*). Thus, RVCaB was subjected to analysis to determine whether RVCaB is indeed an IUP, and was predicted to be IUP by most of the programs tested including FoldIndex (*9*), DisEMBL 1.4 (*10*), DISOPRED 2 (*11*) and IUPred (*12*), but not GlobPlot 2.1 (*13*).

RVCaB has more than 10 Ca^{2+} binding capacity per molecule with low affinity at the mM level, in contrast to the known CaBPs (*19*). In the elucidation of the Ca^{2+} binding mode, there are very few clues as to how the RVCaB protein can bind so many Ca^{2+} ions at such a low affinity, because of its uniqueness both in its Ca^{2+} binding character and the primary structure predicted to be an IUP. In this study, we measured the physico-chemical properties of RVCaB and the thermodynamic characteristics of its interaction with Ca^{2+} to understand the physico-chemical properties of RVCaB Ca^{2+} binding, and found that there is no detectable typical secondary structure such as an α-helix or β-sheet, but rather, a substantial left-handed polyproline type II (PPII) helix in the far-UV circular dichroism (CD) spectra of RVCaB (*20*, *21*). Calorimetric analyses confirmed the high Ca^{2+} binding capacity of RVCaB. Here, we discuss the secondary structural mode of CaBP with a unique primary structure and unique Ca^{2+} binding behaviour based on these physico-chemical properties.

MATERIALS AND METHODS

Plasmid Construction and Protein Overexpression—To determine the physico-chemical properties using a large quantity of highly purified RVCaB, we prepared recombinant protein. The cDNA for wild-type RVCaB was prepared as described previously (*14*). The cDNA was then directly amplified by polymerase chain reaction (PCR) using the primers: 5′-CGGAATTCGATGGCTAC CGCTGACGTTG-3′ and 5′-ATGCGGCCGCCTCATCAG CCTTCTCCACG-3′ (the *Eco*RI and *Not*I sites are underlined). PCR was performed using KOD-Plus DNA polymerase (Toyobo Biochemicals). The amplified DNA fragment was cloned into the vector pZErO^{TM}-2 (Invitrogen). The resulting vector was digested and ligated into the *Eco*RI/*Not*I site of a pET23b expression vector (Novagen). All constructs were sequenced to verify the absence of PCR errors and then the expression vector was introduced into *Escherichia coli* BL21(DE3) (Novagen). Transformants were grown in LB broth at 30°C for 3 h after induction with 0.4 mM isopropyl-1-thio-β-D-galactoside.

Protein Purification—*Escherichia coli* cells expressing RVCaB were harvested by centrifugation and resuspended in 20 mM Tris-acetate (pH 7.5) containing 20% (v/v) glycerol, 0.2 mg ml^{-1} DNase I, 0.4 mg ml^{-1} lysozyme, 10 mM 2-mercaptoethanol and a protein inhibitor cocktail (0.5× Complete, EDTA-free) (Roche Applied Science). The cells were disrupted by sonication for 12.5 min on ice. After removal of cell debris by centrifugation at 104,000 × *g* for 30 min, the supernatant was applied to a Ni-NTA Superflow column (Qiagen) equilibrated with 20 mM imidazole containing 20 mM Tris-acetate (pH 7.5), 20% (v/v) glycerol and 2 M NaCl. RVCaB was eluted with 300 mM imidazole containing 20 mM Tris-acetate (pH 7.5) and 2 M NaCl. The peak fractions were collected and applied to a HiTrap Phenyl HP column (Amersham Biosciences) equilibrated with 20 mM Tris-acetate (pH 7.5) and 2 M NaCl. The protein was recovered in the flow-through fraction. After desalting, the protein was applied to a Sephacryl S-300 HR gel filtration column (Amersham Biosciences). The purified protein was subjected to protein quantification using the BCA protein assay kit (Pierce Biotechnology) (*22*), SDS-PAGE (*23*), Stains-all staining (*14*), MALDI-TOF mass spectroscopy using Voyager-DE PRO (Applied Biosystems) and analytical gel filtration chromatography using a Superdex 200 10/300 GL column (Amersham Biosciences) were performed. There is a tendency to underestimate the RVCaB content by the colorimetric assay and UV analysis, because the protein has a unique amino-acid composition. To verify the accurate content of RVCaB, we weighed the purified RVCaB dried under decompression.

To monitor the structure of RVCaB, a tryptophan residue was introduced into the wild-type RVCaB. The valine residue at position 136 or 202 was exchanged with a tryptophan residue. These mutant RVCaB proteins (V136W and V202W) were also expressed in *E. coli* and purified by column chromatography, the same as the wild-type RVCaB.

$^{45}Ca^{2+}$ Overlay Assay—The effect of heat treatment on Ca^{2+} binding of RVCaB was determined by $^{45}Ca^{2+}$ overlay assay (*14*, *24*). RVCaB with or without heat treatment was slot-blotted onto a polyvinylidene fluoride (PVDF) membrane. The heat treatment of RVCaB was performed at 95°C for 10 min. The membrane was then subjected to $^{45}Ca^{2+}$ overlay assay with 3.7 MBq $^{45}Ca^{2+}$ as $CaCl_2$. Calmodulin (0.2 μg) and immunoglobulin (2 μg) were also applied to the membrane as a positive and a negative control, respectively.

Circular Dichroism Spectroscopy and Dynamic Light Scattering—The ellipticity was followed with a J-725 spectropolarimeter (Jasco) equipped with a PTC-348WI temperature controller (Jasco). The concentrations of protein samples applied were 13 μM for the wild-type and V136W and 12 μM for V202W in 10 mM Tris-HCl (pH 7.5). Far-UV CD spectra of samples (0.5 ml) were measured at a range of 190–250 nm with a light path length of 1 mm. All spectra are shown as the average of five scans. The background signal for the buffer was subtracted from that of the sample spectra. Measurement of the dynamic light scattering (DLS) was performed using DynaPro (Protein Solutions) at 25°C. Before the measurement, the protein solution in 10 mM Tris-acetate (pH 7.5) was centrifuged for 10 min at 20,000 × *g* and filtered through a 0.1 μm Ultrafree-MC filter (Millipore).

Thermodynamics—Differential scanning calorimetry (DSC) was performed using a capillary differential scanning calorimeter VP-CAPILLARY DSC (MicroCal) at a scan rate of 100°Ch^{-1}. Proteins were dissolved in 10 mM Tris-HCl (pH 7.5). Isothermal titration calorimetry (ITC) was performed using an isothermal

titration calorimeter VP-ITC (MicroCal). Prior to the measurements, the solution of RVCaB was dialysed against 20 mM HEPES-KOH (pH 8.0). RVCaB was diluted with the same buffer and then degassed in a vacuum. Five microlitres of 25 mM $CaCl_2$ was injected into a 1.405 ml sample cell containing 82 μM (for WT and V136W) and 79 μM (for V202W) of RVCaB at 25°C. The data were analysed using DSC/ITC data analysis modules in ORIGIN software version 7.0 (MicroCal).

The enthalpy change (ΔH), the association constant (K_a) and the stoichiometry (n) were determined using the ITC titration curve of the binding of Ca^{2+} to RVCaB, and the free energy difference (ΔG) and the entropy difference (ΔS) on Ca^{2+} binding was then calculated from Eq. (1) as follows,

$$\Delta G = -RT \ln K_a = \Delta H - T\Delta S \quad (1)$$

where, R represents the gas constant and T the absolute temperature.

Introduction of Intrinsic Spectroscopic Probe and Fluorescence Measurements—For spectroscopic analysis, Val^{136} or Val^{202} was substituted with a tryptophan residue by site-directed mutagenesis (*25*) with two pairs of primers: 5′-GAGGAAGAATGGGAAGAAACA-3′ (forward) and 5′-GCTAGTTATTGCTCAGCGG-3′ (reverse) for Trp^{136}; 5′-TAATACGACTCACTATAGGG-3′ (forward) and 5′-TGTCTTCTTCCATTCTTCCTC-3′ (reverse) for Trp^{202} (the mutated sites are underlined). The PCR was performed using KOD-Plus DNA polymerase (Toyobo Biochemicals). The obtained DNAs were sequenced to verify the absence of PCR errors. The fluorescence emission spectra of the RVCaB mutants (2 μM of a protein in 10 mM Tris-HCl, pH 7.5) were collected with a Shimadzu RF-5300PC fluorescence spectrophotometer under continuous stirring in an argon atmosphere. The excitation wavelength was set at 277 nm with a bandwidth of 5 nm. The emission spectra were recorded with a bandwidth of 5 nm. The data were analysed using ORIGIN software (MicroCal).

Interpretation of Calcium Dependent Fluorescence Change—The calcium concentration-dependent fluorescence intensity change of the RVCaB mutants was interpreted by the following equations (see Discussion section).

The Ca^{2+} binding of RVCaB,

$$\mathrm{RVCaB} + \mathrm{Ca}^{2+} \leftrightarrows \mathrm{RVCaB} : \mathrm{Ca}^{2+}$$

is written as the equation,

$$K_d = \frac{[\mathrm{RVCaB}][\mathrm{Ca}^{2+}]}{[\mathrm{RVCaB} : \mathrm{Ca}^{2+}]} \quad (2)$$

where, K_d is the dissociation constant of [RVCaB:Ca^{2+}]. Since the fluorescence intensity change ($F_0 - F$) is proportional to [RVCaB:Ca^{2+}] (*26*, *27*), Eq. (3) can be written as follows,

$$F_0 - F = \frac{\Delta F^{spec}_{max}[\mathrm{Ca}^{2+}]_0}{K^{spec}_d + [\mathrm{Ca}^{2+}]_0} \quad (3)$$

where, ΔF^{spec}_{max} is the maximum fluorescence change observed when the protein is fully occupied at the specific Ca^{2+} binding sites with an affinity of K^{spec}_d in a binding site independent manner. $[Ca^{2+}]_0$ is the added Ca^{2+} concentration to the protein solution for the fluorescence measurement. The validity of Eq. (3) was confirmed by the linearity of the plot of $[Ca^{2+}]_0/(F_0 - F)$ versus $[Ca^{2+}]_0$, but there was no linear correlation between them.

Here, we introduced an additional non-specific binding term into Eq. (3), as follows,

$$F_0 - F = \frac{\Delta F^{spec}_{max}[\mathrm{Ca}^{2+}]_0}{K^{spec}_d + [\mathrm{Ca}^{2+}]_0} + \frac{\Delta F^{non}_{max}[\mathrm{Ca}^{2+}]_0}{K^{non}_d + [\mathrm{Ca}^{2+}]_0} \quad (4)$$

This introduction is reasonable, because the highly acidic RVCaB may bind to Ca^{2+} non-specifically. The measured data were analysed by Eq. (4) using a non-linear least square curve fitting with ORIGIN software (MicroCal). The validity of Eq. (4) was confirmed by applying the K^{spec}_d and K^{non}_dvalues obtained from the fluorescence emission data of V202W to that of V136W (see Discussion section for details).

The fluorescence quenching experiments (*26*) of the introduced tryptophan residue in the proteins were analysed using the Stern–Volmer plots (Eq. 5) (*28*).

$$\frac{F_0}{F} = 1 + K_{SV}[Q] \quad (5)$$

where, F_0 and F are the fluorescence intensities in the absence or presence, respectively, of a given concentration of quencher [Q] and K_{SV} is the Stern–Volmer quenching constant.

In the case of the Cs^+ quenching experiments, the results could be analysed using the correction term α of the increment fraction by Cs^+ binding, similar to the Ca^{2+} binding equation of Eq. (3) in the Stern–Volmer equation (Eq. 5);

$$\frac{F_0}{[(1+\alpha) \times \mathrm{F}]} = 1 + K_{SV}[\mathrm{Cs}^+] \quad (5')$$

Thus,

$$\frac{F_0}{F} = (1+\alpha)(1 + K_{SV}[\mathrm{Cs}^+]) \quad (6)$$

where,

$$\alpha = \frac{1}{\Delta F^{bind}([\mathrm{Cs}^+])} \times \frac{\Delta F^{bind}_{max}[\mathrm{Cs}^+]_0}{K_d + [\mathrm{Cs}^+]_0}$$

The non-specific binding second term of Eq. (4) was not considered due to experimental errors, whereas the experimental points were deviated.

RESULTS

Is RVCaB an Unstructured Protein?—The bioinformatic information suggests that RVCaB, which consists of 248 amino-acid residues, is an unstructured protein as described in the Introduction. To study the structural and physicochemical characteristics of RVCaB, a large quantity of the recombinant protein was prepared. The purified recombinant RVCaB exhibited slow migration during SDS-PAGE (Fig. 1A) due to its hydrodynamic and acidic properties (calculated pI, 4.8) (*14*), but this was not sufficient to characterize RVCaB as an intrinsically unordered protein. In the present study, we determined

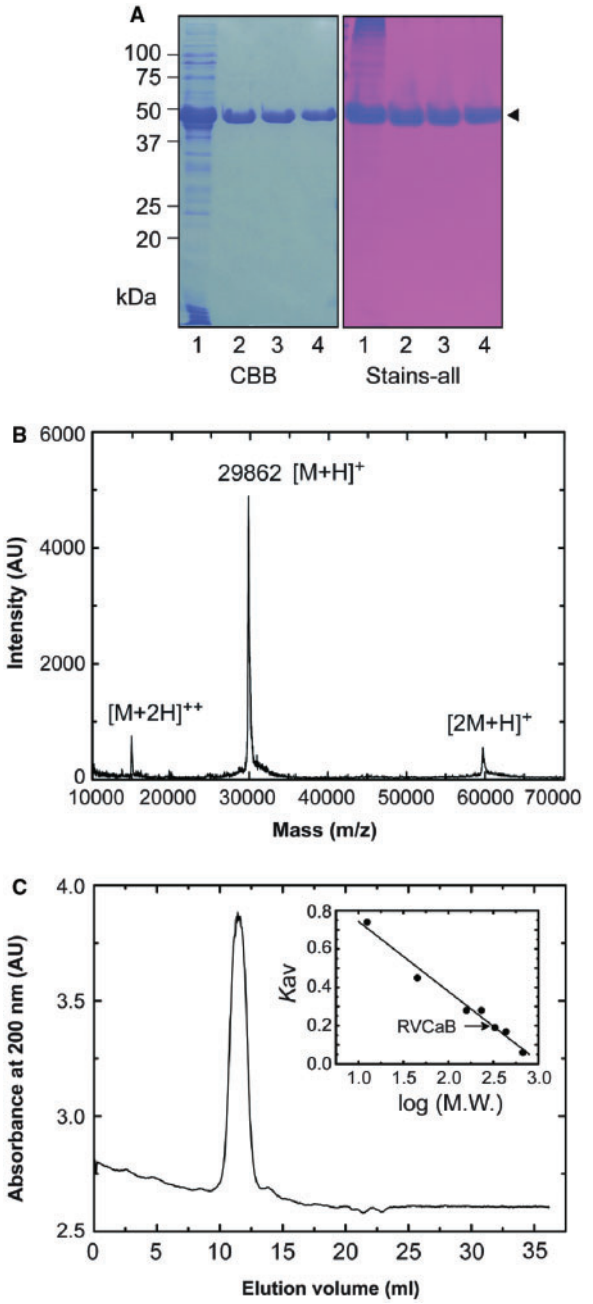

Fig. 1. **Purification (A), mass spectrometry (B) and analytical gel filtration (C) of RVCaB.** (A) RVCaB was expressed in *E. coli* cells and purified from the soluble fraction. Protein samples were subjected to SDS-PAGE and stained with Coomassie brilliant blue (CBB, left panel) or Stains-all (right). Lane 1, soluble fraction (10 μg) prepared from *E. coli* expressing RVCaB; lane 2, preparation (2 μg) after Ni-NTA Superflow column chromatography; lane 3, the flow-through fraction (2 μg) of HiTrap Phenyl HP column chromatography; and lane 4, the peak fraction (2 μg) after Sephacryl S-300 HR column chromatography. (B) Purified RVCaB was applied to MALDI-TOF mass spectrometry. (C) Purified RVCaB (157 μg) was applied to a Superdex200 column equilibrated in 10 mM Tris-acetate (pH 7.5) and 150 mM NaCl. The UV absorption at 200 nm was monitored. The flow rate was maintained at 0.8 ml min^{-1}. Inset, K_{AV} was plotted against the molecular weight of standard globular proteins.

Table 1. **Stokes radius of RVCaB and its mutant proteins determined by dynamic light scattering.**

	None		10 mM $CaCl_2$	
	R_H[a] (nm)	Polydispersity	R_H[a] (nm)	Polydispersity
WT	5.0	20%	5.7	33%
V136W	5.1	23%	5.3	21%
V202W	4.9	23%	5.3	23%

[a]Stokes radii (R_H) were determined for the wild-type RVCaB and two mutant proteins (V136W and V202W) in the presence or absence of 10 mM $CaCl_2$ by dynamic light scattering.

the detailed biophysical properties of RVCaB by mass spectroscopy, size-exclusion chromatography and dynamic light scattering (DLS) experiments. The molecular weight of RVCaB was estimated by the MALDI-TOF mass spectroscopy to 29,862, which was consistent with the theoretical value of RVCaB without the N-terminal methionine residue (29,907) (Fig. 1B). By the analytical gel-filtration column chromatography the molecular weight of RVCaB was calculated to be 330,000 (Fig. 1C), which is 11-times greater than that obtained from mass spectroscopy. The apparent Stokes radius (R_H) determined by DLS measurement was estimated to be 5.0 nm, with a polydispersity of 20% (Table 1). This value is relative to the 143 kDa it would be as a globular protein. These observations suggest that RVCaB lacks the typical compact globular structure.

DSC Measurement of RVCaB—To elucidate whether there was a characteristic protein fold, RVCaB was applied to differential scanning calorimetry (DSC) (Fig. 2), since the DSC is used to investigate the protein folding by monitoring cooperative structural transition to the unfolded state caused by heat denaturation of the protein. When the DSC measurements of RVCaB repeated twice using the same sample, the DSC curve was reproduced (data not shown). The concentration dependency of the gradual transition of the specific heat capacity (C_p) was detected for RVCaB, whereas the lysozyme, a standard protein found as a globular folded protein, showed a clear structural transition at around 59°C. This may reflect the gradual unfolding of RVCaB (Fig. 2A). Regardless of the presence or absence of $CaCl_2$, the DSC curves for RVCaB showed no sharp transition of excess heat capacity up to 110°C (Fig. 2B). Therefore, RVCaB is highly hydrated and has a lack of highly cooperative folding transitions (*29*), while there is small but significant decrease of heat capacity in the Ca^{2+}binding to RVCaB (Fig. 2B).

Secondary Structure of RVCaB—Far-UV CD spectrum changes were measured in a temperature range of 20°C to 99°C to elucidate the temperature-dependent unfolding of the secondary structure of RVCaB (Fig. 3A), and the CD spectrum of RVCaB after cooling to 20°C was restored to the initial spectrum (data not shown). The spectra lacked the typical signatures of secondary structures of the α-helix and β-structure, except for a negative strong signal at 198 nm that is typically found in unstructured proteins and peptides (*30*, *31*). A weak negative peak at 220 nm was also observed in the spectra of RVCaB. Many unstructured proteins (*2*, *3*), including the highly acidic protein, prothymosin α (calculated pI, 3.5) (*4*), have a similar CD feature. As the temperature

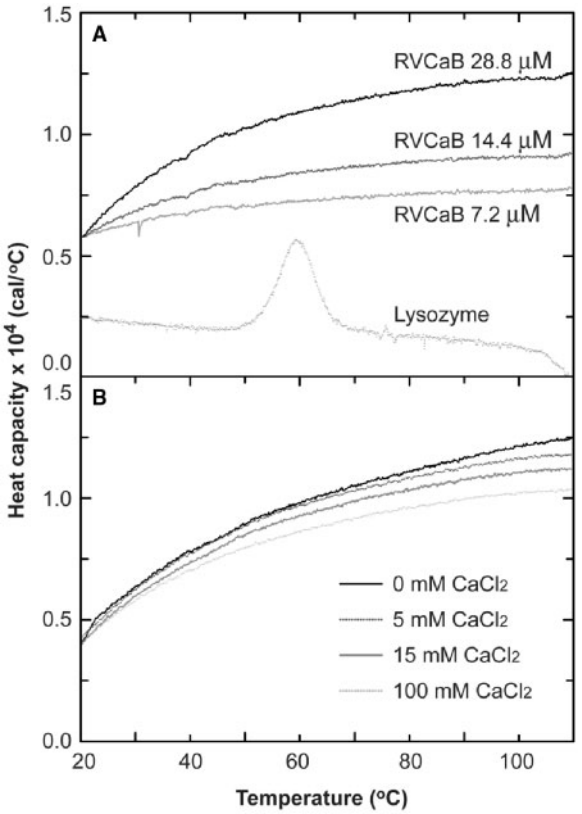

Fig. 2. **Differential scanning calorimetry of RVCaB.** (A) DSC thermograms of RVCaB (protein concentration, 7.2–28.8 μM) and lysozyme (29 μM) as the reference of a globular protein. (B) DSC thermograms of RVCaB (concentration, 29 μM) were recorded in the presence of $CaCl_2$ at different concentrations (0–100 mM). The heating rate was 100°C h^{-1} in 10 mM Tris-HCl (pH 7.5). Curves mean the dependence of excess heat capacity, C_p. The curves of each scan are offset for clarity.

was increased from 20°C to 99°C, the ellipticity at 220 nm was gradually increased as well as a concomitant decrease in the intensity at 198 nm (Fig. 3A). The values of molar ellipticity at 220 and 208.4 nm were plotted as a function of temperature (Fig. 3B). The molar ellipticity at 220 nm decreased linearly as the temperature increased. In contrast, the value at 208.4 nm was maintained at a constant level of −7,100 degree $cm^2\,dmol^{-1}$ in a wide range of temperatures, suggesting that there is an isodichroic point at 208.4 nm. The isodichroic point means a linear combination of the structural transitions between the two conformational states.

The different CD spectra of RVCaB between 20°C and 99°C displayed two peaks at 198 and 220 nm (Fig. 3C). The presence of a positive band at 220 nm indicates that the contribution of α-helical structures to the CD spectrum is absent or very low. These CD spectrum features resemble those of peptides rich in PPII structures (*21*, *29*, *30*, *32–34*). The different CD spectrum of RVCaB in the presence and absence of Ca^{2+} (Fig. 3D) was similar to that of the heat-induced change (Fig. 3C). These results suggest that heat treatment and Ca^{2+}-binding induced a similar structural change in RVCaB.

The Ca^{2+}-binding ability of RVCaB after heat-treatment was confirmed by $^{45}Ca^{2+}$ overlay assay (Fig. 4). There was no difference in the intensity of the bound $^{45}Ca^{2+}$ even after heat treatment of RVCaB at 95°C for 10 min.

Thermodynamic Parameters for RVCaB—ITC measurements were performed at 25°C and pH 8.0 to examine the thermodynamic features of the interaction of RVCaB with Ca^{2+}. In the calorimetric titration, the binding of Ca^{2+} to RVCaB is endothermic (Fig. 5A). The sum of the heat absorption by each injection, which was normalized by the concentration of RVCaB (Fig. 5B), and the titration curves fitted well to a model of n identical binding sites with the same affinity (see Materials and methods section). The K_a value from the ITC measurement (360 M^{-1}; this work) agrees with the value obtained previously by the equilibrium dialysis method (294 M^{-1}) (*19*). The determined thermodynamic parameters indicate that the Ca^{2+}-binding process to RVCaB is an entropy-driven phenomenon (Table 2), and the entropic contribution ($-T\Delta S = -7.2$ kcalmol^{-1} at 298 K or 25°C) compensates for the positive enthalpy change, ($\Delta H = 3.7$ kcal·mol^{-1}), resulting in favourable Ca^{2+} binding with a negative free energy change, ($\Delta G = -3.5$ kcal·mol^{-1}).

Binding Mode Analysis of RVCaB—Two mutant proteins of RVCaB were prepared to elucidate the binding mode of Ca^{2+}. A tryptophan residue was introduced into RVCaB as an intrinsic fluorescent probe at the 136 position located at the middle of four repeat sequences (V136W) or at the 202 position located in the C-terminal region (V202W). Each preparation of purified mutant protein was displayed as a single protein band on SDS-PAGE (Fig. 6A) and an absorption peak of around 280 nm in the UV absorption spectrum (Fig. 6B). Thus, we used these preparations as the purified mutant proteins.

The thermodynamic parameters for the mutants were determined to investigate the effect of the mutation (Table 2). The ΔG values of both of the RVCaB mutants for Ca^{2+} binding were almost the same as that of the wild-type. However, the stoichiometry (Ca^{2+} per protein) was decreased from 21.6 to 13.6 for V136W and to 11.2 for V202W, respectively. The other thermodynamic values, ΔH and $T\Delta S$, were increased to similar values in both mutants. The Stokes radii for the mutants determined by DLS were almost the same as those of the wild-type RVCaB (Table 1), and the same hydrodynamic result was also obtained by analytical gel filtration (data not shown).

The fluorescence emission spectra of the mutants V136W and V202W exhibited emission maxima at 355 and 354 nm, respectively (Fig. 6C), although there was a difference in the intensity between the two mutants. The fluorescence intensities of the mutants were increased in V202W and decreased in V136W, when the calcium concentration was increased (Fig. 6D). These observations indicate that tryptophan residues are exposed to the solvent in different micro-environments in the V136W and V202W mutants (*26*, *35*).

The fluorescence quenching experiment by acrylamide, which quenches the fluorescence of the exposed and

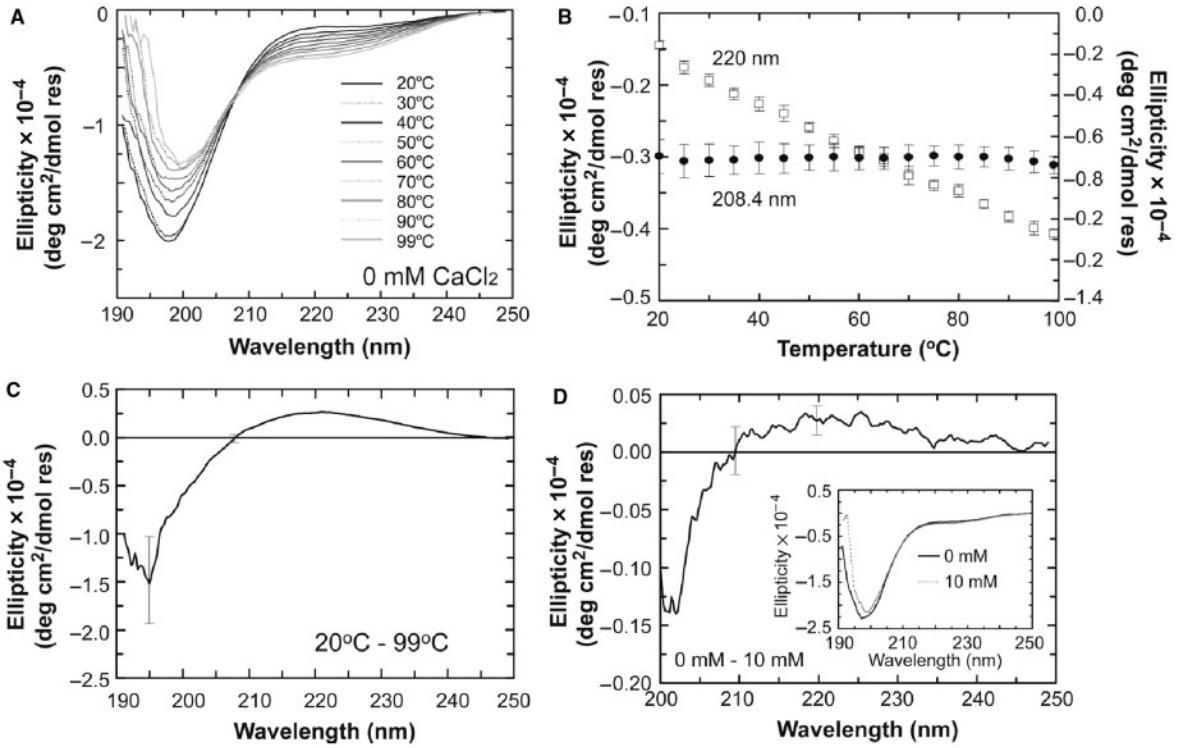

Fig. 3. **Far-UV CD spectrum analysis of the secondary structure in RVCaB.** (A) Effect of temperatures on the structure of RVCaB. Far-UV CD spectra in 10 mM Tris-HCl (pH 7.5), were obtained every 10°C from 20°C to 99°C. An apparent isodichroic point was at 208.4 nm. (B) Gradual conformational spectrum change induced by heating from 20°C to 99°C. The ellipticity ([θ]) at 220 nm (open squares) and 208.4 nm (closed circles) was plotted against the temperature. (C) Different CD spectrum of RVCaB between 20°C and 99°C (20°C minus 99°C). (D) Effect of Ca^{2+} on the secondary structure in RVCaB. Different CD spectrum of RVCaB between the absence and presence of 10 mM $CaCl_2$ (at 0 mM minus at 10 mM) was plotted against the wavelength. Inset, Far-UV CD spectra in 10 mM Tris-HCl (pH 7.5) were obtained with (dashed lines) and without 10 mM $CaCl_2$ (solid lines). Traces were smoothed using 11-point adjacent averaging. The estimated error is shown by the error bars.

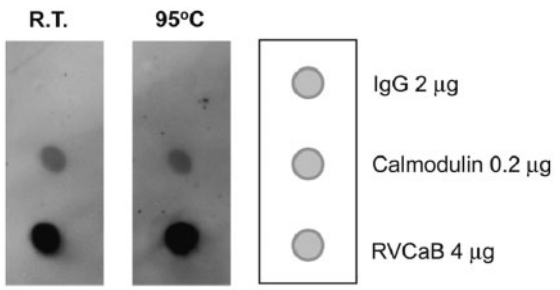

Fig. 4. **Effect of heat treatment on the Ca^{2+} binding property of RVCaB.** The purified RVCaB (with or without heat treatment) was slot-blotted onto a polyvinylidene fluoride membrane, and then the membrane was subjected to $^{45}Ca^{2+}$ overlay assay. RVCaB was heated at 95°C for 10 min and then applied to a membrane (middle panel). IgG (a negative control) and calmodulin (a positive control) were not subjected to heat-treatment in either case (both cases).

buried tryptophan residue in proteins as a non-ionic quencher (*26*), was performed for both mutants with and without 10 mM $CaCl_2$. All the Stern–Volmer plots are on the same line regardless of the presence or absence of the Ca^{2+} ion at moderate concentrations (0 to 30 mM) of acrylamide and the same Stern–Volmer value is, $K_{SV} = 19.1\,M^{-1}$, in the acrylamide-quenching of RVCaB regardless of the presence of Ca^{2+} (Fig. 6E) (*28*), suggesting that the dynamic accessibility of the non-ionic quencher, acrylamide, to the tryptophan residue in RVCaB was very high, but not affected by the bound Ca^{2+}. Next, cesium chloride (CsCl) quenching of the mutants was performed as an ionic quencher, and the non-linearity in the Stern–Volmer plot was observed in the absence of Ca^{2+}, but a simple linear pattern in the presence of 10 mM $CaCl_2$ (Fig. 6F). This could be fitted using the Stern–Volmer equation with a modification with the same fluorescent effects for the calcium binding [Eq (6) in Materials and methods section], whereas it could not be analysed with modified Stern–Volmer or static quenching by CsCl. The binding of Cs^+ ions to RVCaB in the absence of Ca^{2+} contributes to the fluorescence change as with the Ca^{2+} binding (Fig. 6D) as well as the usual dynamic quenching by the Cs^+ ion, since it is consistent that the fluorescent quenching by Cs^+ followed the Stern–Volmer equation (5) in the presence of Ca^{2+} due to the occupation of the specific binding sites by the added 10 mM Ca^{2+} (Fig. 6F).

These quenching experiments suggest that: (i) the dynamic quenching by a non-ionic quencher has the

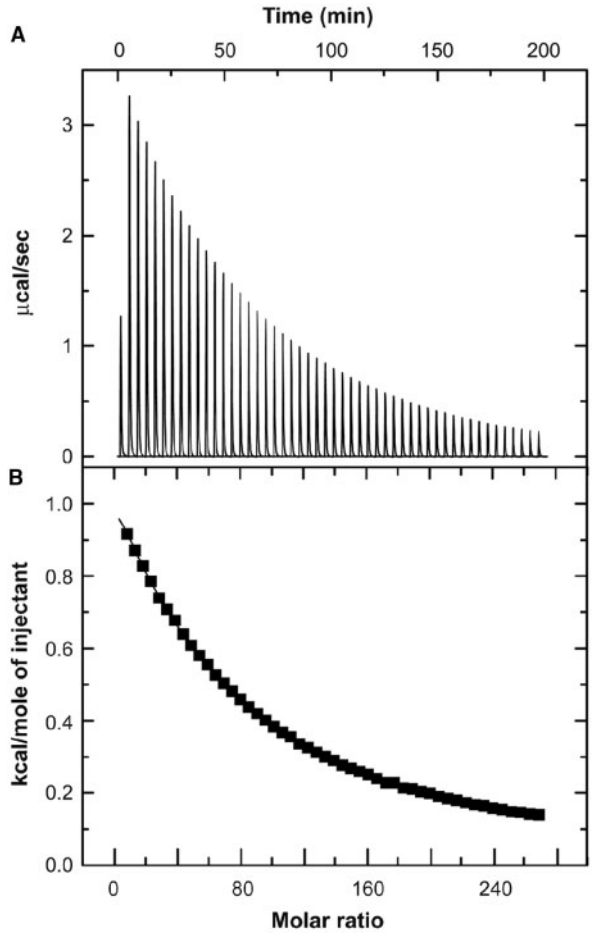

Fig. 5. **Isothermal titration calorimetry for the association of Ca^{2+} with RVCaB.** (A) A typical raw titration curve for the Ca^{2+} binding monitored by ITC. (B) Integration of the thermogram yielded a binding isotherm. The solid line represents the non-linear regression of the data points according to a model of *n* identical binding sites with the same affinity (see text for details). The parameters K_a, *n* and ΔH upon Ca^{2+} binding obtained are summarized in Table 2.

same effect on the conformational change of the RVCaB mutants in both Ca^{2+}-bound and unbound forms. (ii) The binding of Cs^+ as well as the ionic quencher induces a similar conformational change to the Ca^{2+} binding in the absence of Ca^{2+}. The dynamic quenching of the RVCaB mutants are consistent with the reported highly exposed tryptophan residues (*36*), as shown by both the fluorescence emission maxima and high Stern–Volmer values, while the solvent accessibility for Trp^{136} in V136W and Trp^{202} in V202W are different but in similar modes, as judged by the quenching studies.

Interestingly, small changes in DLS (Table 1), far-UV CD spectrum (Fig. 3D), and fluorescence (Fig. 6D) were observed on the binding of Ca^{2+}. In contrast to these parameters, the heat capacities of the DSC measurements decreased with the increase of the Ca^{2+} binding to RVCaB. The present observations suggest a very small structural rearrangement but rather distinct hydration modes of RVCaB in the presence or absence of the Ca^{2+} ion, which may be substituted by other cations because of the absence of consensus results in the various physicochemical measurements among DLS, far-UV CD, DSC and the introduced intrinsic fluorescent probe, and the fact there is no change in the structural cooperativity at all.

DISCUSSION

Basal Structure of RVCaB with the Polyproline Type II Helix—The CD spectrum analyses of RVCaB did not reveal a typical α-helix or β-strand conformation (Fig. 3). We also examined the effect of SDS and a chaotrope guanidine hydrochloride (GdnHCl) in the CD spectra of RVCaB. Neither 1% SDS nor 2 M GdnHCl modified the CD spectra (data not shown), suggesting that RVCaB is highly hydrated in the native state. In general proteins such as RVCaB without a typical secondary structure except for a PPII type helix are categorized as being natively unfolded, unordered or unstructured proteins (*1*, *7*).

On the other hand, DSC analysis suggests a gradually unfolding of RVCaB under high temperatures (Fig. 2). Furthermore, the detailed CD analysis gave a clue to estimating the higher-order structure. Changes in CD spectra over a range of temperatures suggest temperature-dependent structural transitions in RVCaB. The protein showed a peak at around 220 nm in different far-UV CD spectra between low and high temperatures (Fig. 3C). The spectrum is similar to that observed for the peptides with a left-handed PPII helix (*20*, *29*). The PPII helix is also known as a collagen chain conformation. RVCaB contains 22 proline residues (8% of the total residues). The proline content of RVCaB is not especially high, but the PPII helix is often also observed in proline-poor peptides (*37*, *38*) that include tri-glutamic acid, tri-aspartic acid, tri-lysine (*39*), hepta-lysine (*40*), tri-alanine (*41*), tetra-alanine (*42*) or hepta-alanine sequences (*38*). Also, proteins with larger polylysine, polyglutamic acid and polyaspartic acid sequences have been reported to contain PPII helices (*30*, *43*). RVCaB has a single tetra-alanine, a single tetra-glutamic acid, two tri-alanine and 12 tri-glutamic acid sequences (*14*). Thus it is reasonable that RVCaB has significant PPII helical content.

The present observations suggest that the temperature-dependent CD spectrum change was due to an extension of the PPII helix in RVCaB by the temperature increment (Fig. 3). The amount of PPII helix can be calculated roughly according to the following equation introduced by Park *et al*. (*21*)

$$[\theta]_{222} = +9580 f_{PPII} - 5560 f_u$$

where, f_{PPII} represents the fraction of the PPII helix and f_u the fraction of the unstructured form. The calculated PPII content of RVCaB based on the thermal structural transition was 25%. This estimation represents a minimum estimate because the presence of even a small amount of α-helical structure would significantly decrease the estimation of the PPII structure. The remaining part of RVCaB may be in the unfolded structure. The PPII content in RVCaB was reduced to 10% when heated at 99°C.

Table 2. **Thermodynamic parameters of the association of Ca^{2+} with RVCaB and its mutant proteins.**

Protein	n (Ca^{2+}/RVCaB)	K_a (M^{-1})	ΔG (kcal mol^{-1})	ΔH (kcal mol^{-1})	$-T\Delta S$ (kcal mol^{-1})
WT	21.6 ± 1.9	360 ± 5.9	−3.5	3.7 ± 0.3	−7.2
WT[a]	19	294			
V136W	13.6 ± 1.7	417 ± 7.0	−3.6	5.0 ± 0.7	−8.4
V202W	11.2 ± 1.4	442 ± 6.2	−3.6	5.7 ± 0.7	−9.3

[a]The data from the equilibrium dialysis method (*19*).

The presence of the PPII helix in RVCaB is consistent with its large Stokes radius (5.0 nm). The value is relative to a 143 kDa globular protein, although the molecular mass was determined to be 29,862 by mass analysis (Fig. 1B). The apparent molecular size of RVCaB was calculated to be 330 kDa by analytical gel-filtration column chromatography using a globular protein standard (Fig. 1C). These results of RVCaB are compatible with the hydrodynamic character of a highly hydrated, long fibrous structure and we propose that RVCaB exists as a monomer or oligomer (dimer or trimer) of the extended polypeptide with a PPII type helix as an intrinsically unfolded protein (IUP). Thus, it was reasonable that we failed in our effort to prepare crystals of the RVCaB protein for X-ray crystallography, since it is likely impossible to crystallize RVCaB as an IUP in its natural state.

Structural Features of Ligand-binding and Ligand-free RVCaB—The content of the PPII helix was slightly decreased when incubated with 10 mM $CaCl_2$ (Fig. 3D) and was calculated to be 23%. The PPII helix has no hydrogen bond between the residues and is a flexible structure. Therefore, Ca^{2+}-binding does not alter the structure of RVCaB markedly, although a small change was detected (Fig. 3D). The sequences of Ala_3, Ala_4, Glu_4 and Glu_3 in RVCaB are the most likely candidates for the formation of the PPII helices and Ca^{2+}-binding sites. Therefore, the extended PPII helices may provide an advantage to RVCaB for the binding of a large number of Ca^{2+} ions. Low affinity for Ca^{2+} of RVCaB may be also owing to intrinsically unfolded structure of RVCaB, which prevents the formation of sterically restrained Ca^{2+}-binding pocket with high affinity like calmodulin.

The PPII helix has been reported to be involved in protein–protein interactions. For example, the PPII helix fits structurally with the ligand-binding site of the Src homology 3 (SH3) domain (*44*). Thus, there is a possibility that PPII helices in RVCaB may play a role in calcium signaling in the vacuole by interacting with a partner protein, although here is no report concerning an interactive protein with RVCaB at present.

Thermodynamic Parameters of Ligand Binding—The thermodynamic parameters indicate that the Ca^{2+} binding to RVCaB is an entropy-driven reaction (Table 2). This is explained by the partial unfolding of the PPII helices and dehydration of the helices and ions. Because of their charge, both RVCaB and Ca^{2+} are highly hydrated in water. On the binding of Ca^{2+} to RVCaB, hydrated water molecules would be released from both the ion and the protein, and this would increase the entropy. Entropy increase on ligand binding ($T\Delta S$, ~7.2 kcal mol^{-1} at 25°C) has also been reported for an organic chelator (*45*) and for the Ca^{2+} binding site introduced into a human lysozyme with hydration changes but no significant conformational change, since the crystallographic studies confirmed that no conformational disorder occurred by the binding of Ca^{2+} in the lysozyme (*46*). In both cases, the increase in entropy was explained as due to the release of the water molecules bound to Ca^{2+} and proteins (*45*, *46*). Thus, we speculate that the entropy-driven ligand binding is a common reaction for proteins which do not change their conformation markedly.

When a tryptophan residue was inserted into RVCaB to monitor the micro-environmental changes around the introduced indole ring, the number of Ca^{2+} bound to the protein was decreased to 13.6 for V136W and 11.2 for V202W from 21.6 in the wild-type (Table 2), although the Stokes radii of these proteins were unchanged regardless of the presence or absence of Ca^{2+} (Table 1). The insertion sites of the tryptophan residue are adjacent to the tri-glutamic acid sequence. Thus substitution with the tryptophan residue would disturb the highly hydrated structure in the vicinity of the large hydrophobic aromatic indole ring in the mutant proteins so as to decrease the capacity for Ca^{2+} binding. The PPII helix content of the mutant proteins was not decreased in far-UV CD spectra (data not shown), and there was also no change in the Stokes radius.

Ligand-induced Structural Change of RVCaB—The fluorescence intensity of the RVCaB mutants (V136W and V202W) was changed in a calcium concentration dependent manner (Fig. 6D). We explain the reason for this change by the specific and non-specific calcium binding effect model shown in Eq. (4) in the 'Materials and methods' section. The titration curve of V202W was fitted to the theoretical line of the model (the line shown in Fig. 6D) and allowed us to extract the biochemical parameters of RVCaB. The K_d^{spec} and K_d^{non} values were 0.8 and 29 mM, respectively. The K_d^{spec} value obtained here agreed with the value obtained by ITC measurement (2.8 mM). Since the high K_d value (>10 mM) is not feasibly detected by ITC measurement, and we could not detect the contribution of the non-specific Ca^{2+} binding in the ITC thermogram (Fig. 5). It is reasonable for the K_d^{non} value to come from non-specific binding of Ca^{2+} in the highly acidic RVCaB shown in the fluorescent studies (Fig. 6D). To examine the validity of this interpretation, we applied the obtained K_d^{spec} and K_d^{non} values in the V202W experiment to the fluorescent titration of V136W in the analysis. The model fitted to the titration curve of V136W without inconsistency, when the parameters K_d^{spec} and K_d^{non} of the same values in V202W were applied in Eq. (4).

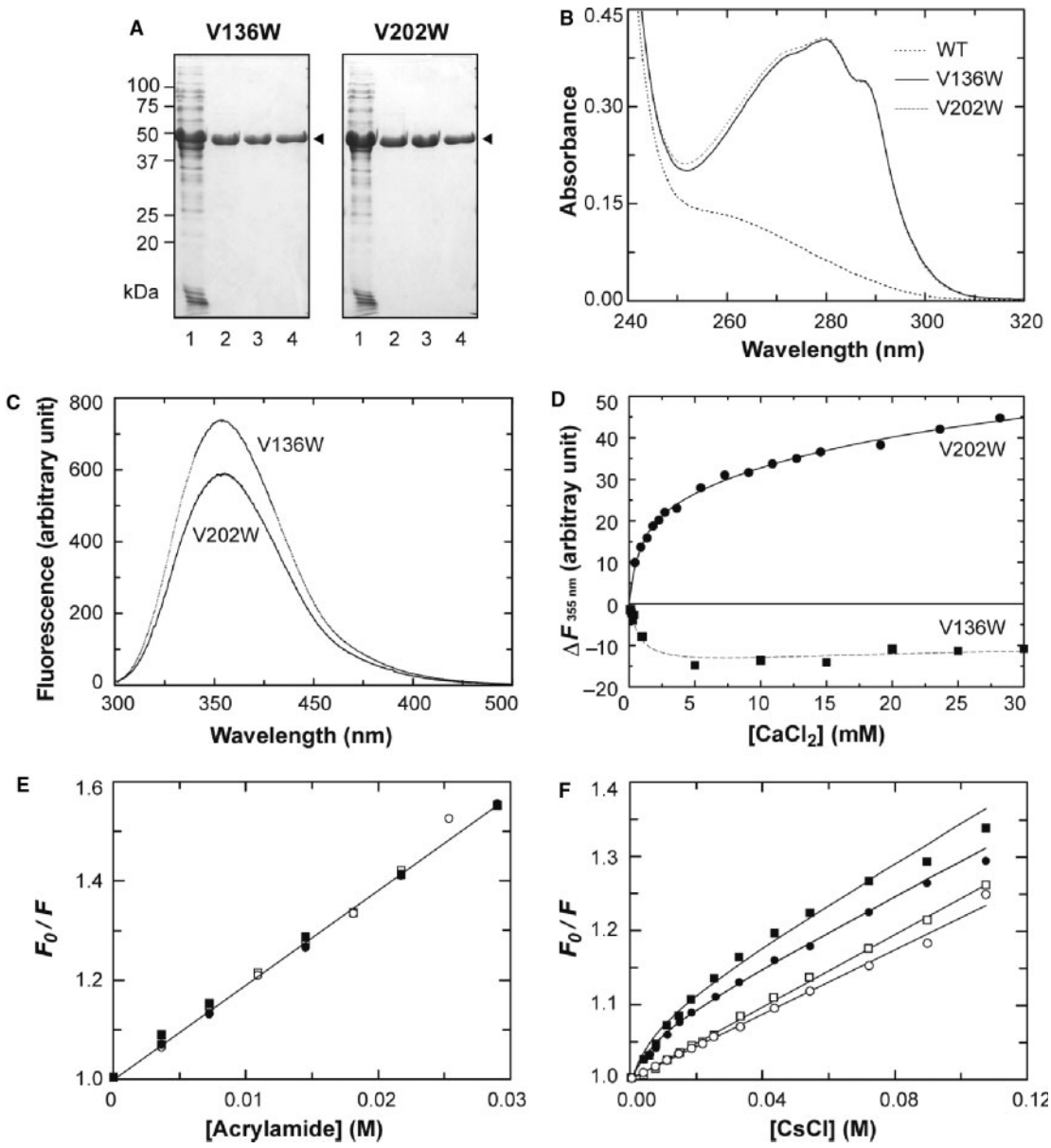

Fig. 6. **Preparation and fluorescence emission spectra of RVCaB mutant proteins.** (A) The RVCaB mutant proteins V136W and V202W were expressed in *E. coli* cells and purified from the soluble fraction. Protein samples were subjected to SDS-PAGE and stained with Coomassie brilliant blue. Lane 1, soluble fraction (10 μg) prepared from *E. coli* expressing RVCaB; lane 2, preparations (2 μg) after Ni-NTA Superflow column chromatography; lane 3, the flow-through fraction (2 μg) of HiTrap Phenyl HP column chromatography; and lane 4, the purified fraction (2 μg) after Sephacryl S-300 HR column chromatography. (B) UV absorption spectra of wild-type and two mutant (V136W and V202W) proteins in 10 mM Tris-HCl (pH 7.5). (C) Fluorescence emission spectra of V136W and V202W. (D) Calcium-concentration dependence of fluorescence at 355 nm for V136W (closed squares) and V202W (closed circles). The solid and dashed lines represent theoretical curves of Ca^{2+}-dependent fluorescence change (see text). (E and F) Stern–Volmer plots for fluorescence quenching of V136W (open and closed squares) and V202W (open and closed circles) by the non-ionic quencher, acrylamide (E), and the ionic quencher, cesium (F), with (open squares and open circles) or without 10 mM $CaCl_2$ (closed squares and closed circles). The ratio F_0/F was plotted against (a) the quencher concentration. Solid lines represent the calculated curves of (F_0/F) using the obtained Stern–Volmer constants in the presence of 10 mM Ca^{2+} ion (F). In the case of the absence of the Ca^{2+} ion, the fluorescent changes by Cs^+ concentrations were analysed by a combination of the specific Cs^+ binding to RVCaB and the Stern–Volmer quenching by the Cs^+ ion (see text) (F).

In conclusion, RVCaB, which is rich in glutamic-acid residues, does not have a definitive protein fold and is an intrinsically unstructured protein for the most part, possessing substantially a PPII helical structure. The present study revealed that the extended PPII helices and intrinsically unfolded structure of RVCaB supports its high capacity for binding Ca^{2+}. Many unstructured and partly unstructured proteins undergo structural change by ligand binding and are frequently involved in important regulatory functions in the

cell (*47*). RVCaB also slightly but significantly changes its structure by Ca^{2+} binding, which has a high content in the PPII helical structure (Fig. 3D), but marked structural cooperativity did not arise by ligand binding in DSC (Fig. 2B). RVCaB is a unique protein that has no intrinsically defined structure except for the PPII helices regardless of the presence or absence of Ca^{2+}, although it cannot be ruled out that RVCaB forms a certain definitive structure in the case of binding to some as yet unidentified binding protein. These properties may be reflective of the calcium-sequestering function of RVCaB with the high capacity of Ca^{2+}-binding in the vacuoles of plant cells. Extensive studies on human titin, a giant structural protein in striated muscle sarcomeres, revealed that the PPII helices in titin provide an elastic structure (*48*) and interaction sites with Src homology domain 3 (*49*). Titin, with its elastic, clustered PPII helices has been proposed to be a signal integration protein, which acts both as a stress sensor and actuator. Although there is at present no evidence that RVCaB functions as a signal-transducing molecule in plant cells, the possibility is worthy of future investigation.

We thank Drs S. Kuramitsu and A. Ebihra for kindly allowing us to use ITC equipment, Drs K. Yutani and M. Sawano for characterizing the thermal stability of RVCaB and Drs K. Takio and M. Nakamura for determining the mass spectroscopic molecular weight of RVCaB. We also thank Mr Y. Nakamura for supporting this work. We also thank Dr Y. Nakanishi and Mr Y. Ide (Nagoya University) for help in preparation of recombinant RVCaB. Financial support of the Ministry of Education, Sports, Culture, Science and Technology of Japan (to M. Maeshima), the Global Research Program (Korea) to M. Maeshima, and The Japan Science Society (to N.N.) is gratefully acknowledged. Pacific Edit reviewed the article prior to submission.

REFERENCES

1. Fink, A.L. (2005) Natively unfolded proteins. *Curr. Opin. Struc. Biol.* **15**, 35–41
2. Sanchéz-Puig, N., Veprintsev, D.B., and Fersht, A.R. (2005) Human full-length securin is a natively unfolded protein. *Protein Sci.* **14**, 1410–1418
3. Schweers, O., Schonbrunn-Hanebeck, E., Marx, A., and Mandelkow, E. (1994) Structural studies of tau protein and Alzheimer paired helical filaments show no evidence for β-structure. *J. Biol. Chem.* **269**, 24290–24297
4. Gast, K., Damaschun, H., Eckert, K., Schulze-Forster, K., Maurer, H.R., Muller-Frohne, M., Zirwer, D., Czarnecki, J., and Damaschun, G. (1995) Prothymosin alpha: a biologically active protein with random coil conformation. *Biochemistry* **34**, 13211–13218
5. Anfinsen, C.B. (1973) Principles that govern the folding of protein chains. *Science* **181**, 223–230
6. Receveur-Brechot, V., Bourhis, J.M., Uversky, V.N., Canard, B., and Longhi, S. (2006) Assessing protein disorder and induced folding. *Proteins* **62**, 24–45
7. Dunker, A.K., Brown, C.J., Lawson, J.D., Iakoucheva, L.M., and Obradovic, Z. (2002) Intrinsic disorder and protein function. *Biochemistry* **41**, 6573–6582
8. Uversky, V.N., Gillespie, J.R., and Fink, A.L. (2000) Why are "natively unfolded" proteins unstructured under physiologic conditions? *Proteins* **41**, 415–427
9. Prilusky, J., Felder, C.E., Zeev-Ben-Mordehai, T., Rydberg, E.H., Man, O., Beckmann, J. S., Silman, I., and Sussman, J. L. (2005) Foldindex©: a simple tool to predict whether a given protein sequence is intrinsically unfolded. *Bioinformatics* **21**, 3435–3438
10. Linding, R., Jensen, L.J., Diella, F., Bork, P., Gibson, T.J., and Russell, R.B. (2003) Protein disorder prediction: implications for structural proteomics. *Structure* **11**, 1453–1459
11. Ward, J. J., Sodhi, J. S., McGuffin, L. J., Buxton, B. F., and Jones, D. T. (2004) Prediction and functional analysis of native disorder in proteins from the three kingdoms of life. *J. Mol. Biol.* **337**, 635–645
12. Dosztányi, Z., Csizmók, V., Tompa, P., and Simon, I. (2005) The pairwise energy content estimated from amino acid composition discriminates between folded and intrinsically unstructured proteins. *J. Mol. Biol.* **347**, 827–839
13. Linding, R., Russell, R.B., Neduva, V., and Gibson, T.J. (2003) GlobPlot: exploring protein sequences for globularity and disorder. *Nucleic Acids Res.* **31**, 3701–3708
14. Yuasa, K. and Maeshima, M. (2000) Purification, properties, and molecular cloning of a novel Ca^{2+}-binding protein in radish vacuole. *Plant Physiol.* **124**, 1069–1078
15. Sanders, D., Brownlee, C., and Harper, J.F. (1999) Communicating with calcium. *Plant Cell* **11**, 691–706
16. Sanders, D., Pelloux, J., Brownlee, C., and Harper, J.F. (2002) Calcium at the crossroads of signaling. *Plant Cell* **14**, S401–S417
17. Yuasa, K. and Maeshima, M. (2001) Organ specificity of a vacuolar Ca^{2+}-binding protein RVCaB in radish and its expression under Ca^{2+}-deficient conditions. *Plant Mol. Biol.* **47**, 633–640
18. Tompa, P. (2002) Intrinsically unstructured proteins. *Trends Biochem. Sci.* **27**, 527–533
19. Yuasa, K. and Maeshima, M. (2002) Equilibrium dialysis measurements of the Ca^{2+}-binding properties of recombinant radish vacuolar Ca^{2+}-binding protein expressed in *Escherichia coli*. *Biosci. Biotechnol. Biochem.* **66**, 2382–2387
20. Makarov, A.A., Lobachov, V.M., Adzhubei, I.A., and Esipova, N.G. (1992) Natural polypeptide in left-handed helical conformation: a circular dichroism study of the linker histones' C-terminal fragments and β-endorphin. *FEBS Lett.* **306**, 63–65
21. Park, S.H., Shalongo, W., and Stellwagen, E. (1997) The role of PPII conformations in the calculation of peptide fractional helix content. *Protein Sci.* **6**, 1694–1700
22. Smith, P.K., Krohn, R.I., Hermanson, G.T., Mallia, A.K., Gartner, F.H., Provenzano, M.D., Fujimoto, E.K., Goeke, N.M., Olson, B.J., and Klenk, D.C. (1985) Measurement of protein using bicinchonic acid. *Anal. Biochem.* **150**, 76–85
23. Laemmli, U.K. (1970) Cleavage of structural proteins during the assembly of the head of bacteriophage T4. *Nature* **227**, 680–685
24. Maruyama, K., Mikawa, T., and Ebashi, S. (1984) Detection of calcium binding proteins by ^{45}Ca autoradiography on nitrocellulose membrane after sodium dodecyl sulfate gel electrophoresis. *J. Biochem.* **95**, 511–519
25. Kirsch, R.D. and Joly, E. (1998) An improved PCR-mutagenesis strategy for two-site mutagenesis or sequence swapping between related genes. *Nucleic Acids Res.* **26**, 1848–1850
26. Pain, R.H. (1998) Determining the fluorescence spectrum of a protein in *Current Protocols in Protein Science* (Coligan, J. E., Dunn, B. M., Speicher, D. W. and Wingfield, P. T., eds.) Unit 7.7, John Wiley & Sons, New York
27. Ohnishi, M., Yamashita, T., and Hiromi, K. (1977) Static and kinetic studies by fluorometry on the interaction

between gluconolactone and glucoamylase from *Rh. niveus*. *J. Biochem.* **81**, 99–105
28. Stern, O. and Volmer, M. (1919) Über die abklingungszeit der fluoreszenz. *Phys. Z.* **20**, 183–188
29. Soulages, J.L., Kim, K., Arrese, E.L., Walters, C., and Cushman, J.C. (2003) Conformation of a group 2 late embryogenesis abundant protein from soybean: evidence of poly (L-proline)-type II structure. *Plant Physiol.* **131**, 963–975
30. Woody, R.W. (1992) Circular dichroism and conformation of unordered peptides. *Adv. Biophys. Chem.* **2**, 37–79
31. Shi, Z., Woody, R.W., and Kallenbach, N.R. (2002) Is polyproline II a major backbone conformation in unfolded proteins? *Adv. Protein Chem.* **62**, 163–240
32. Soulages, J.L., Kim, K., Walters, C., and Cushman, J.C. (2002) Temperature-induced extended helix/random coil transitions in a group 1 late embryogenesis-abundunt protein from soybean. *Plant Physiol.* **128**, 822–832
33. Fox, D.G., Cary, P.D., and Kneale, G.G. (1999) Conformational studies of the C-terminal domain of bacteriophage Pf1 gene 5 protein. *Biochim. Biophys. Acta* **1435**, 138–146
34. Bienkiewicz, E.A., Woody, M.A.Y., and Woody, R.W. (2000) Conformation of the RNA polymerase II C-terminal domain: circular dichroism of long and short fragments. *J Mol. Biol.* **297**, 119–133
35. Hlodan, R. and Pain, R.H. (1994) Tumor necrosis factor is in equilibrium with a trimeric molten globule at low pH. *FEBS Lett.* **343**, 256–260
36. Pokalsky, C., Wick, P., Harms, E., Lytle, F.E., and Van Etten, R.L. (1995) Fluorescence resolution of the intrinsic tryptophan residues of bovine protein tyrosyl phosphatase. *J. Biol. Chem.* **270**, 3809–3815
37. Chen, Y.H., Yang, J.T., and Martinez, H.M. (1972) Determination of the secondary structures of proteins by circular dichroism and optical rotatory dispersion. *Biochemistry* **11**, 4120–4131
38. Shi, Z., Olson, C.A., Rose, G.D., Baldwin, R.L., and Kallenbach, N.R. (2002) Polyproline II structure in a sequence of seven alanine residues. *Proc. Natl Acad. Sci. USA* **99**, 9190–9195
39. Eker, F., Griebenow, K., Cao, X., Nafie, L.A., and Shweitzer-Stenner, R. (2004) Tripeptides with ionizable side chains adopt a perturbed polyproline II structure in water. *Biochemistry* **43**, 613–621
40. Rucker, A.L. and Creamer, T.P. (2002) Polyproline II helical structure in protein unfolded states: lysine peptides revisited. *Protein Sci.* **11**, 980–985
41. Cao, X., Nafie, L., and Shweitzer-Stenner, R. (2002) Tripeptides adopt stable structures in water. A combined polarized visible Raman, FTIR, and VCD spectroscopy study. *J. Am. Chem. Soc.* **124**, 14330–14341
42. Shweitzer-Stenner, R., Eker, F., Griebenow, K., Cao, X., and Nafie, L. (2004) The conformation of tetraalanine in water determined by polarized Raman, FT-IR, and VCD spectroscopy. *J. Am. Chem. Soc.* **126**, 2768–2776
43. Smyth, E., Syme, C.D., Blanch, E.W., Hecht, L., Vasak, M., and Barron, L.D. (2001) Solution structure of native proteins with irregular folds from Raman optical activity. *Biopolymers* **58**, 138–151
44. Rath, A., Davidson, A.R., and Deber, C.M. (2005) The structure of "unstructured" regions in peptides and proteins: role of the polyproline II helix in protein folding and recognition. *Biopolymers* **80**, 179–185
45. Charles, R.G. (1954) Heats and entropies of reaction of metal ions with ethylenediaminetetraacetate. *J. Am. Chem. Soc.* **76**, 5854–5858
46. Kuroki, R., Kawakita, S., Nakamura, H., and Yutani, K. (1992) Entropic stabilization of a mutant human lysozyme induced by calcium binding. *Proc. Natl Acad. Sci. USA* **89**, 6803–6807
47. Wright, P.E. and Dyson, H.J. (1999) Intrinsically unstructured proteins: re-assessing the protein structure-function paradigm. *J. Mol. Biol.* **293**, 321–331
48. Ma, K., Kan, L., and Wang, K. (2001) Polyproline II helix is a key structural motif of the elastic PEVK segment of titin. *Biochemistry* **40**, 3427–3438
49. Ma, K., Forbes, J.G., Gutierrez-Cruz, G., and Wang, K. (2006) Titin as a giant scaffold for integrating stress and Src homology domain 3-mediated signaling pathways. *J. Biol. Chem.* **281**, 27539–27556